JASA ARTICLE

A spherical expansion for audio sounds generated by a circular parametric array loudspeaker

Jiaxin Zhong,[a] Ray Kirby,[b] and Xiaojun Qiu[c]
Centre for Audio, Acoustics and Vibration, Faculty of Engineering and Information Technology, University of Technology Sydney, New South Wales 2007, Australia

ABSTRACT:
The existing non-paraxial expression of audio sounds generated by a parametric array loudspeaker (PAL) is hard to calculate due to the fivefold integral in it. A rigorous solution of the Westervelt equation under the quasilinear approximation is developed in this paper for circular PALs by using the spherical harmonics expansion, which simplifies the expression into a series of threefold summations with uncoupled angular and radial components. The angular component is determined by Legendre polynomials and the radial one is an integral involving spherical Bessel functions, which converge rapidly. Compared to the direct integration over the whole space, the spherical expansion is rigorous, exact, and can be calculated efficiently. The simulations show the proposed expression can obtain the same accurate results with a speed of at least 15 times faster than the existing one.
 https://doi.org/10.1121/10.0001261
(Received 1 April 2020; revised 28 April 2020; accepted 28 April 2020; published online 15 May 2020)
[Editor: Nail A. Gumerov] Pages: 3502–3510

I. INTRODUCTION

Parametric array loudspeakers (PALS) are an application of the parametric acoustic arrays for radiating highly directional audio sounds in air with the carrier wave of ultrasounds.[1] PALS have been used in many applications such as active noise control systems,[2] personal communications,[3] measurements of the acoustic parameters of materials,[4] and mobile robotic navigation,[5] where calculation of the audio sounds generated by a PAL is important.

When a PAL radiates two intensive ultrasound (primary) waves at different frequencies, a secondary wave containing the difference-frequency wave (the audio sound in air) is generated due to the nonlinearity. The nonlinear interactions of primary waves are rather complex, and some approximations and simplifications have to be made in the mathematical modelling. The simplest model assumes the ultrasound waves are collimated and fully attenuated in the nearfield and the audio sound is generated by a line array of virtual audio sources with the exponentially decreased source strength along the radiation axis of the PAL. The Khokhlov–Zabolotskaya–Kuznetsov (KZK) equation considers the diffraction, absorption, and nonlinearity of this phenomenon under the parabolic approximation, and many methods have been proposed to solve the KZK equation analytically or numerically; but the results are usually only valid within the paraxial region about 20° from the transducer axis.[6]

The sound pressure at wide angles can be predicted based on the Westervelt equation, and it is considered in this paper.[7,8] The quasilinear approximation is assumed because the ultrasound level generated by a PAL is limited for safety concerns.[1] In this model, the ultrasounds are calculated first with the Rayleigh integral, i.e., a twofold integral over the area of the transducer surface. Then, an infinitely large volume source is constructed with its source density function being proportional to the product of the sound pressure of ultrasounds. Finally, the audio sound is calculated by integrating the sound pressure generated by the volume source over the whole space. This solution is a fivefold integral and hard to compute. The Gaussian beam expansion (GBE) method is widely used to simplify the calculation by transforming the twofold integral for the ultrasounds into a onefold summation.[9]

The GBE method approximates the vibration velocity profile of the transducer surface with a set of Gaussian ones to simplify the ultrasound expression thanks to the simplicity of Gaussian beams under the Fresnel (high frequency) approximation.[10] Although the GBE method uses less calculation time than the direct integration of the Rayleigh integral, it is not an exact solution of the Westervelt equation under the quasilinear approximation. Furthermore, Gibbs oscillations occur for a uniform piston source no matter how many Gaussian beams are used,[9,10] and the calculation of the off-axis audio sound is slow due to the triple-integral over the whole space.

In this paper, a simplified but rigorous solution of the Westervelt equation under the quasilinear approximation for a circular PAL is developed by using spherical harmonics expansion. The key is to express the Green function of a point monopole in free space as a series of trigonometric, Legendre, and spherical Bessel functions. The integrals in the expression of the audio sounds are then eliminated using

[a]Electronic mail: Jiaxin.Zhong@student.uts.edu.au, ORCID: 0000-0002-9972-8004.
[b]ORCID: 0000-0002-3520-1377.
[c]ORCID: 0000-0002-5181-1220.

https://doi.org/10.1121/10.0001261

the orthogonal properties of the trigonometric and Legendre functions. Compared to direct integration over the whole space, spherical expansion is rigorous, exact, and can be calculated efficiently. Similar techniques have been used in the other literatures for calculating sound radiation from a baffled piston,[11] rotating sources,[12] ring sources,[13] and resilient and rigid disks.[14]

II. THEORY

As shown in Fig. 1, a circular PAL with the radius of a generates two harmonic ultrasounds at frequencies f_1 and f_2 ($f_1 > f_2$) and the boundary condition on the transducer surface is

$$v_z(\rho_s, t) = v_1(\rho_s)e^{-j\omega_1 t} + v_2(\rho_s)e^{-j\omega_2 t}, \tag{1}$$

where j is the complex unit, v_z represents the vibration velocity normal to the transducer surface, ρ_s is the distance of the surface source point $\mathbf{r}_s$ to the center of the PAL, $v_i(\rho_s)$, the amplitude of the vibration velocity at ρ_s, is assumed to be axisymmetric about the radiation axis, and $\omega_i = 2\pi f_i$ ($i = 1, 2$) is the angular frequency of the ith primary wave.

The radiation of the PAL is governed by the well known Westervelt equation,[7]

$$\nabla^2 p - \frac{1}{c_0^2}\frac{\partial^2 p}{\partial t^2} = -\frac{\delta}{c_0^4}\frac{\partial^3 p}{\partial t^3} - \frac{\beta}{\rho_0 c_0^4}\frac{\partial^2 p^2}{\partial t^2}, \tag{2}$$

where p is the sound pressure and c_0 is the linear sound speed. The first term on the right-hand side accounts for the fluid thermo-viscosity, where δ is the sound diffusivity parameter, which relates to the atmospheric sound attenuation coefficient α at the angular frequency ω by $\alpha(\omega) = \omega^2\delta/(2c_0^3)$.[15] The second term on the right-hand side accounts for the nonlinearity where ρ_0 is the static fluid density and β is the nonlinearity coefficient.

The solutions of the ultrasounds and audio sound with the frequency $f_a = f_1 - f_2$ are denoted as

$$\tilde{p}_i(\mathbf{r}, t) = p_i(\mathbf{r})e^{-j\omega_i t}, \ i = 1, 2, \text{a}, \tag{3}$$

where the subscripts "1," "2," and "a" represent the two ultrasounds and the audio sound, respectively, $\mathbf{r} = (x, y, z)$ is a field point location, the rectangular coordinate system

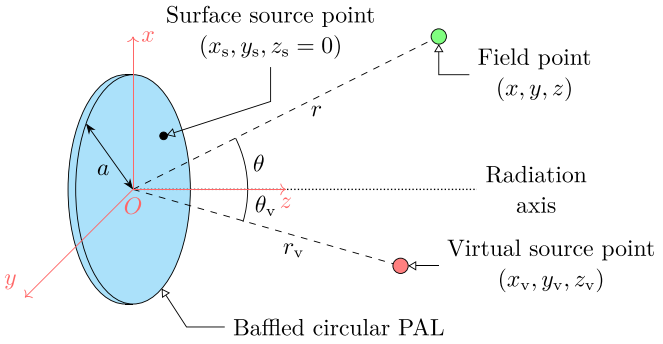

FIG. 1. (Color online) Sketch of a baffled circular PAL.

O-xyz is established centered at the center of the PAL, and the axis z is normal to the transducer surface.

Because the ultrasound level generated by a PAL is limited due to safety concerns, the nonlinearity is weak and the quasilinear approximation can be used in the derivation.[1] For the PAL placed on an infinitely large baffle, the audio sound can be treated as the superposition of the sounds generated by infinitely many virtual sources at $\mathbf{r}_v = (x_v, y_v, z_v)$ and their image sources at $(x_v, y_v, -z_v)$.[8] By using the successive method, the sound pressure of the audio sound is[8]

$$p_a(\mathbf{r}) = -j\rho_0\omega_a\int_{-\infty}^{\infty}\int_{-\infty}^{\infty}\int_{-\infty}^{\infty} q(\mathbf{r}_v)\frac{e^{jk_a d_v}}{4\pi d_v}dx_v dy_v dz_v, \quad z > 0, \tag{4}$$

where the complex audio wavenumber $k_a = \omega_a/c_0 + j\alpha_a$, α_a is the sound attenuation coefficient in air at frequency f_a, $d_v = \sqrt{(x - x_v)^2 + (y - y_v)^2 + (z - z_v)^2}$ is the distance between the field point $\mathbf{r}$ and the virtual source point or its image, and the source density function is[16]

$$q(\mathbf{r}_v) = -\frac{j\beta\omega_a}{\rho_0^2 c_0^4}p_1(\mathbf{r}_v)p_2^*(\mathbf{r}_v), \tag{5}$$

which is symmetric about the transducer surface, i.e., $q(x_v, y_v, -z_v) = q(x_v, y_v, z_v)$.

The sound pressure of the ultrasounds can be obtained by the Rayleigh integral as[8]

$$p_i(\mathbf{r}_v) = -2j\rho_0\omega_i\int_0^{2\pi}\int_0^a \frac{e^{jk_i d_s}}{4\pi d_s}v_i(\rho_s)\rho_s d\rho_s d\varphi_s, \tag{6}$$

where the complex ultrasonic wavenumber $k_i = \omega_i/c_0 + j\alpha_i$, α_i is the sound attenuation coefficient at frequency f_i, $i = 1$ and 2, $d_s = \sqrt{(x_v - x_s)^2 + (y_v - y_s)^2 + z_v^2}$ is the distance between the virtual source point $\mathbf{r}_v$ and the source point $\mathbf{r}_s = (x_s, y_s, z_s = 0)$ on the transducer surface, $x_s = \rho_s\cos\varphi_s$, and $y_s = \rho_s\sin\varphi_s$. Equation (4) is an exact solution of the Westervelt equation under the quasilinear approximation but is hard to be calculated numerically due to the fivefold integral after substituting Eqs. (5) and (6) into it.[8]

The GBE method can simplify the calculation by transforming the twofold integral Eq. (6) into a onefold summation,[9]

$$p_i(\mathbf{r}_v) = \rho_0 c_0 v_{i,0}\sum_{g=1}^{G}\frac{A_g}{1 + jB_g z_v/R_i} \times e^{\left[-B_g/(1+jB_g z_v/R_i)\right]\left[(x_v^2/a^2)+(y_v^2/a^2)\right]+jk_i z_v}, \tag{7}$$

where the Rayleigh distance $R_i = k_i a^2/2$, $i = 1, 2$, A_g and B_g are the GBE coefficients and G is the GBE number, and $v_{i,0}$ is a constant determined by the velocity profile $v_i(\rho_s)$ and GBE coefficients. The GBE parameters A_g, B_g, and G are obtained by the heuristic method where the transducer vibration velocity profile is approximated by the superposition of

several (G) Gaussian velocity profiles. For a circular piston source where $v_i(\rho_s) = v_{i,0}$, the expansion coefficients have been calculated for $G = 10$,[9] $G = 15$,[17] $G = 25$,[18] or $G = 40$,[10] where larger G provides more accurate results.

The source density function of audio sounds Eq. (5) is transformed into a twofold summation after substituting Eq. (7) into it. By substituting Eq. (5) into Eq. (4), the audio sound pressure can be numerically calculated. For the off-axis field point, which is not located on the radiation axis of the PAL, the threefold integral in Eq. (4) has to be numerically calculated. While for the on-axis field point, $x = y = 0$ and Eq. (4) can be simplified into a twofold integral using the symmetry of the azimuthal angle,[8]

$$p_a(\mathbf{r}) = -2\pi j\rho_0\omega_a \int_{-\infty}^{\infty}\int_0^{\infty} q(\mathbf{r}_v)\frac{e^{jk_a\sqrt{\rho_v^2+(z-z_v)^2}}}{4\pi\sqrt{\rho_v^2+(z-z_v)^2}} \times \rho_v d\rho_v dz_v, \quad z > 0, \tag{8}$$

where $\rho_v^2 = x_v^2 + y_v^2$.

Although the GBE method is faster than the direct integration in Eq. (6), calculating the ultrasound fields at virtual source points in the whole space is still time-consuming. Furthermore, Eq. (7) is not an exact transformation of Eq. (6) and the near field ultrasound pressure calculated by Eq. (7) is hard to make accurate.[10] In Secs. II A and II B, the fivefold integral Eq. (4) is simplified without using any additional approximations.

A. Simplification of ultrasounds

The ultrasound field should be simplified first because it is included in the expression of the audio sound Eq. (4). To simplify the sound pressure of ultrasounds, a spherical coordinate system (r, θ, φ) is established based on the rectangular one (x, y, z), where r, θ, and φ are the radial distance, polar angle, and azimuthal angle, respectively. The Green function in free field, i.e., $g_i(\mathbf{r}_v, \mathbf{r}_s) = e^{jk_i d_s}/(4\pi d_s)$ in Eq. (6), can be expanded under the spherical coordinates as the summation of spherical harmonic terms

$$g_i(\mathbf{r}_v, \mathbf{r}_s) = \frac{jk_i}{4\pi}\sum_{\mu=0}^{\infty}(2\mu+1)h_\mu(k_i r_{vs,>})j_\mu(k r_{vs,<}) \times \sum_{m=-\mu}^{\mu}\frac{(\mu-m)!}{(\mu+m)!}P_\mu^m(\cos\theta_v) \times P_\mu^m(\cos\theta_s)e^{jm(\varphi_v-\varphi_s)}, \tag{9}$$

where (r_v,θ_v, φ_v) and (r_s, θ_s, φ_s) are spherical coordinates of the virtual source point $\mathbf{r}_v$ and the source point on PAL surface $\mathbf{r}_s$, respectively, $r_{vs,<} = \min(r_v, r_s)$, $r_{vs,>} = \max(r_v, r_s)$, $j_\mu(\cdot)$ is the spherical Bessel function, $h_\mu(\cdot) = j_\mu(\cdot) + jy_\mu(\cdot)$ is the spherical Hankel function of the first kind, $y_\mu(\cdot)$ is the spherical Neumann function, $P_\mu^m(\cdot)$ is the associated Legendre function at the degree μ and order m, and $\theta_s = \pi/2$ as shown in Fig. 1.

Substituting Eq. (9) into Eq. (6) and performing the integral with respect to φ_s yields

$$p_i(\mathbf{r}_v) = \rho_0 c_0 \sum_{\mu=0}^{\infty}(2\mu+1)P_\mu(\cos\theta)P_\mu(\cos\theta_s) \times \int_0^a v_i(r_s)h_\mu(k_i r_{vs,>})j_n(k_i r_{vs,<})k_i^2 r_s dr_s, \tag{10}$$

where $r_s = \rho_s$ because $\theta_s = \pi/2$. By using the explicit expression of $P_\mu(0)$ (Eq. 4.2.4 in Ref. 19),

$$P_\mu(\cos\theta_s) = P_\mu(0) = \begin{cases} (-1)^{\mu/2}\dfrac{\Gamma\left(\frac{\mu}{2}+\frac{1}{2}\right)}{\sqrt{\pi}\Gamma\left(\frac{\mu}{2}+1\right)}, & \mu = \text{even} \\ 0, \quad \mu = \text{odd}. \end{cases} \tag{11}$$

After omitting the odd terms and using the substitution $\mu = 2n$, Eq. (10) can be simplified as

$$p_i(\mathbf{r}_v) = \rho_0 c_0 \sum_{n=0}^{\infty} C_n P_{2n}(\cos\theta_v)R_{i,2n}(r_v), \tag{12}$$

where the coefficient and the radial component are

$$C_n = (-1)^n(4n+1)\frac{\Gamma\left(n+\frac{1}{2}\right)}{\sqrt{\pi}\Gamma(n+1)} \tag{13}$$

and

$$R_{i,2n}(r_v) = \begin{cases} h_{2n}(k_i r_v)\displaystyle\int_0^{k_i r_v} v_i(\xi/k_i)j_{2n}(\xi)\xi d\xi \\ +j_{2n}(k_i r_v)\displaystyle\int_{k_i r_v}^{k_i a} v_i(\xi/k_i)h_{2n}(\xi)\xi d\xi, \ r_v < a, \\ h_{2n}(k_i r_v)\displaystyle\int_0^{k_i a} v_i(\xi/k_i)j_{2n}(\xi)\xi d\xi, \quad r_v > a \end{cases} \tag{14}$$

respectively, and $\Gamma(\cdot)$ is the gamma function (Sec. 3.1 in Ref. 19). The inner ($r_v < a$) and outer ($r_v > a$) radial components in Eq. (14) are denoted by $R_{i,2n}^{\text{in}}(r_v)$ and $R_{i,2n}^{\text{outer}}(r_v)$, respectively, for simplicity in the following text. The radial component Eq. (14) is obtained in Ref. 14 in a similar manner. The numerical technique for calculating Eq. (14) is described in Sec. III.

B. Simplification of audio sounds

Equation (4) can be similarly expanded under the spherical coordinates as the summation of spherical harmonic terms

$$p_a(\mathbf{r}) = -j\rho_0\omega_a \int_0^{2\pi}\int_0^{\pi}\int_0^{\infty} q(\mathbf{r}_v)g_a(\mathbf{r}, \mathbf{r}_v)r_v^2 \times \sin\theta_v dr_v d\theta_v d\varphi_v, \ z > 0, \tag{15}$$

where $g_a(\cdot)$ is given by Eq. (9). Substituting Eq. (9) into Eq. (15) and performing the integral with respect to φ_v yields

https://doi.org/10.1121/10.0001261

$$p_a(\mathbf{r}) = \rho_0\omega_a k_a \sum_{\mu=0}^{\infty}\left(\mu+\frac{1}{2}\right)P_\mu(\cos\theta) \times \int_0^{\pi}\int_0^{\infty} q(\mathbf{r}_v)P_\mu(\cos\theta_v)h_\mu(kr_{v,>}) \times j_\mu(kr_{v,<})r_v^2\sin\theta_v \mathrm{d}r_v\mathrm{d}\theta_v, \quad (16)$$

where (r, θ, φ) are spherical coordinates of the field point $\mathbf{r}$, $r_{v,<} = \min(r_v, r)$, and $r_{v,>} = \max(r_v, r)$.

Substituting the source density function Eq. (5) and the simplified ultrasounds Eq. (12) into Eq. (16), it has

$$p_a(\mathbf{r}) = -\mathrm{j}\beta\rho_0 \sum_{l,m,\mu=0}^{\infty} C_l C_m\left(\mu+\frac{1}{2}\right)P_\mu(\cos\theta) \times \left[\int_0^{\pi} P_{2l}(\cos\theta_v)P_{2m}(\cos\theta_v)P_\mu(\cos\theta_v)\sin\theta_v\mathrm{d}\theta_v\right] \times \left[\int_0^{\infty} R_{1,2l}(r_v)R^*_{2,2m}(r_v)h_\mu(k_a r_{v,>})j_\mu(k_a r_{v,>})k_a^3 r_v^2\mathrm{d}r_v\right]. \quad (17)$$

Using the formula for the integral of triple Legendre polynomials [Eq. (11) in Ref. 20],

$$\int_0^{\pi} P_{n_1}(\cos\theta)P_{n_2}(\cos\theta)P_{n_3}(\cos\theta)\sin\theta\mathrm{d}\theta = 2\begin{pmatrix} n_1 & n_2 & n_3 \\ 0 & 0 & 0 \end{pmatrix}^2, \quad (18)$$

Eq. (17) becomes

$$p_a(\mathbf{r}) = -\mathrm{j}\beta\rho_0 \sum_{l,m,\mu=0}^{\infty} C_l C_m(2\mu+1) \times \begin{pmatrix} 2l & 2m & \mu \\ 0 & 0 & 0 \end{pmatrix}^2 P_\mu(\cos\theta) \times \left[\int_0^{\infty} R_{1,2l}(r_v)R^*_{2,2m}(r_v)h_\mu(k_a r_{v,>}) \times j_\mu(k_a r_{v,>})k_a^3 r_v^2\mathrm{d}r_v\right], \quad (19)$$

where $\begin{pmatrix} n_1 & n_2 & n_3 \\ 0 & 0 & 0 \end{pmatrix}$ is the Wigner $3j$ symbol that can be calculated using the formula [Eq. (C.23) in Ref. 21]

$$\begin{pmatrix} n_1 & n_2 & n_3 \\ 0 & 0 & 0 \end{pmatrix} = \begin{cases} 0, & 2n_0 = \text{odd} \\ (-1)^{n_0}\dfrac{n_0!}{(n_0-n_1)!(n_0-n_2)!(n_0-n_3)!} \times \sqrt{\dfrac{(2n_0-2n_1)!(2n_0-2n_2)!(2n_0-2n_3)!}{(2n_0+1)!}}, & 2n_0 = \text{even}, \end{cases} \quad (20)$$

and the triangular inequality should be satisfied, i.e., $|n_1 - n_2| \le n_3 \le n_1 + n_2$, where $2n_0 = n_1 + n_2 + n_3$. The Wigner $3j$ symbol equals to 0 if $n_1 + n_2 + n_3$ is odd. After omitting the odd terms in Eq. (19) and using the substitution $\mu = 2n$, Eq. (19) becomes

$$p_a(\mathbf{r}) = -\mathrm{j}\beta\rho_0 \sum_{l,m,n=0}^{\infty} C_l C_m(4n+1) \times \begin{pmatrix} 2l & 2m & 2n \\ 0 & 0 & 0 \end{pmatrix}^2 P_{2n}(\cos\theta)F_{2l,2m,2n}(r), \quad (21)$$

with the radial component of the audio sounds

$$F_{2l,2m,2n}(r) = \int_0^{\infty} R_{1,2l}(r_v)R^*_{2,2m}(r_v)h_{2n}(k_a r_{v,>}) \times j_{2n}(k_a r_{v,>})k_a^3 r_v^2\mathrm{d}r_v, \quad (22)$$

and explicit expressions for the inner region ($r < a$) and the outer region ($r > \mathrm{a}$) are

$$\begin{aligned} F^{\text{in}}_{2l,2m,2n}(r) &= h_{2n}(k_a r)\int_0^r R^{\text{in}}_{1,2l}(r_v)\left[R^{\text{in}}_{2,2m}(r_v)\right]^* j_{2n}(k_a r_v)k_a^3 r_v^2\mathrm{d}r_v \\ &\times j_{2n}(k_a r)\int_r^a R^{\text{in}}_{1,2l}(r_v)\left[R^{\text{in}}_{2,2m}(r_v)\right]^* h_{2n}(k_a r_v)k_a^3 r_v^2\mathrm{d}r_v \\ &+ j_{2n}(k_a r)\int_a^{\infty} R^{\text{out}}_{1,2l}(r_v)\left[R^{\text{out}}_{2,2m}(r_v)\right]^* \\ &\times h_{2n}(k_a r_v)k_a^3 r_v^2\mathrm{d}r_v, \quad r < a, \end{aligned} \quad (23)$$

and

$$\begin{aligned} F^{\text{out}}_{2l,2m,2n}(r) &= h_{2n}(k_a r)\int_0^a R^{\text{in}}_{1,2l}(r_v)\left[R^{\text{in}}_{2,2m}(r_v)\right]^* \\ &\times j_{2n}(k_a r_v)k_a^3 r_v^2\mathrm{d}r_v + h_{2n}(k_a r) \\ &\times \int_a^r R^{\text{out}}_{1,2l}(r_v)\left[R^{\text{out}}_{2,2m}(r_v)\right]^* j_{2n}(k_a r_v)k_a^3 r_v^2\mathrm{d}r_v \\ &+ j_{2n}(k_a r)\int_r^{\infty} R^{\text{out}}_{1,2l}(r_v)\left[R^{\text{out}}_{2,2m}(r_v)\right]^* h_{2n}(k_a r_v) \\ &\times k_a^3 r_v^2\mathrm{d}r_v, \quad r > a, \end{aligned} \quad (24)$$

respectively. It is shown in Sec. IV that only the outer region of Eq. (24) is required for most scenarios because the inner region is very small compared to the space of interests.

Equation (21) is the main result of this paper. It is an exact solution to the audio sounds generated by a PAL solved by the Westervelt function with the quasilinear assumption. Because no additional assumptions are made in the derivation, it is equivalent rigorously to the original solution Eq. (4) which has fivefold integrals and is more accurate than the GBE solution. Equation (21) can be calculated more efficiently for three reasons. First, it is a series with threefold summation consisting of uncoupled spherical angular and radial components, so it can be calculated quickly for a large number of field points. Second, the radial component $F_{2l,2m,2n}(r)$ can be transformed into a rapidly converged integral using the property of spherical Bessel functions (see

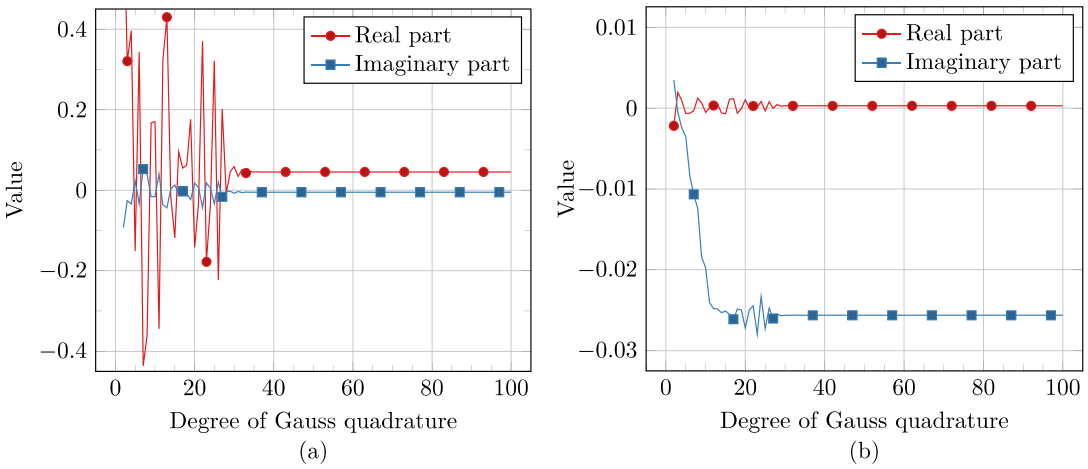

FIG. 2. (Color online) Numerical results of the integral (a) $h_{20}(k_1a)\int_0^{k_1a} j_{20}(\xi)\xi \mathrm{d}\xi$ and (b) $j_{20}(0.1k_1a)\int_{0.1k_1a}^{k_1a} h_{20}(\xi)\xi \mathrm{d}\xi$ using the Gauss−Legendre quadrature.

Sec. III for details). Finally, due to the restrictions of the triangular inequality, many values of Wigner $3j$ symbol are zero, so many terms do not need to be calculated.

III. NUMERICAL TECHNIQUES

The radial component of the sound pressure of ultrasounds Eq. (14) and of audio sounds Eq. (22) involves integrals and can be calculated accurately using the normalized spherical Bessel functions and the complex plane method, respectively. Although the theory is applicable for arbitrary axisymmetric velocity profiles of ultrasounds, they are assumed to be uniform in Secs. III and IV, i.e., $v_i(\rho_s) = v_{i,0}$, $i = 1$ and 2.

A. Radial component of ultrasounds

Two types of definite integrals in Eq. (14) are required to be calculated, which are $h_{2n}(x)\int_0^x j_{2n}(\xi)\xi \mathrm{d}\xi$ and $j_{2n}(x_1)\int_{x_1}^{x_2} h_{2n}(\xi)\xi \mathrm{d}\xi$. In this paper, the Gauss−Legendre quadrature is used to calculate them numerically (Sec. 5.5 in Ref. 22). A typical example is shown in Fig. 2 when $x = 0.1k_1$, $x_1 = 0.01k_1$, and $x_2 = 0.1k_1$, where $k_1 = (1190.7 + 0.297\mathrm{j})/\mathrm{m}$ is obtained using the data in Table I and $a = 0.1$ m. It can be seen that the integration has a fast converge and a degree of 40 is enough to achieve a satisfactory precision.

Although the Gauss−Legendre quadrature is useful for calculating integrals in Eq. (14), it overflows when calculating their integrand $j_{2n}(z_j)$ or $h_{2n}(z_h)$ if the order n is much larger than the absolute value of the argument of the spherical Bessel or Hankel functions, z_j or z_h. To solve the overflow of spherical Bessel and Hankel functions, the normalized versions of them are introduced as[23]

$$\bar{j}_{2n}(z_j) = \frac{(4n+1)!!}{z_j^{2n}} j_{2n}(z_j), \tag{25}$$

and

$$\bar{h}_{2n}(z_h) = \frac{\mathrm{j} z_h^{2n+1}}{(4n-1)!!} h_{2n}(z_h), \tag{26}$$

which can be numerically obtained using the recurrence relations and the MATLAB code package presented in Ref. 23. The normalized spherical Bessel and Hankel functions have the asymptotic behavior,

$$\bar{j}_{2n\to\infty}(z_j) \sim \bar{h}_{2n\to\infty}(z_h) \sim 1 + O(1/n), \tag{27}$$

where $O(\cdot)$ means its quantity has the same magnitude as the one inside the parenthesis. By using the relations Eqs. (25) and (26), the product is rewritten as

TABLE I. The parameters used in the numerical calculations.

Name	Value	Note
Frequencies of ultrasounds	$f_1 = 65$ kHz $f_2 = 64$ kHz	Typical frequencies of the commercial PAL, e.g.: Holosonics Audio Spotlight AS-24i
Audio frequency	$f_a = 1$ kHz	—
Sound attenuation coefficients	$\alpha_1 = 0.30$ Np/m $\alpha_2 = 0.29$ Np/m $\alpha_a = 6.9 \times 10^{-4}$ Np/m	Calculated according to ISO 9613-1 with the relative humidity 60% and temperature 25 °C (Ref. 27)
Transducer surface radius	$a = 0.1$ m	—
Surface vibration velocity amplitude	$v_{1,0} = v_{2,0} = 0.12$ m/s	The sound pressure level (SPL) of ultrasound is about 125 dB at 1 m away on the radiation axis

https://doi.org/10.1121/10.0001261

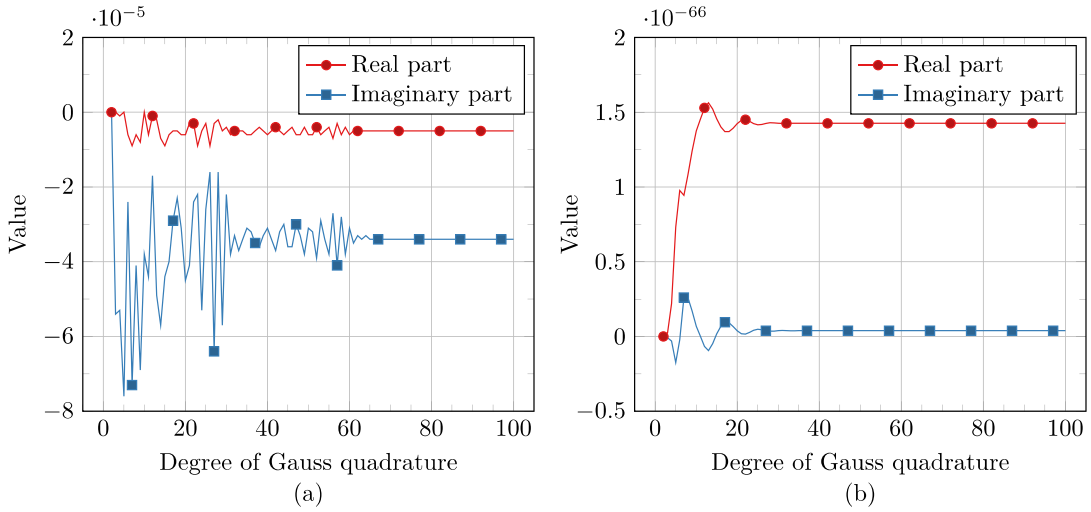

FIG. 3. (Color online) Numerical results of the first term of the outer radial component Eq. (24) when $r = 1$ m for (a) $l = m = n = 0$ and (b) $l = m = n = 30$.

$$j_{2n}(z_j)h_{2n}(z_h) = \frac{1}{\mathrm{j}(4n+1)}\frac{z_j^{2n}}{z_h^{2n+1}}\bar{j}_{2n}(z_j)\bar{h}_{2n}(z_h). \tag{28}$$

B. Radial component of audio sounds

The radial component of audio sounds Eq. (22) contains three terms for both inner and outer regions as shown in Eqs. (23) and (24). The integrals of the first and second term on the right-hand side of Eqs. (23) and (24) are similar and can be calculated with the Gauss−Legendre quadrature. Because the integration range of the third term is from r to ∞, the substitution of the variable to be integrated

$$r_{\mathrm{v}} = \tan\left[\frac{\pi}{4}(\xi+1)\right] + r, \tag{29}$$

is used [Eq. (2.12) in Ref. 24] so that the new variable ξ is integrated over the finite range from -1 to 1. Equation (29) is valid for the outer radial component Eq. (24) while the similar substitution is valid for the inner component Eq. (23) by setting $r = a$ in Eq. (29).

To illustrate the performance of the Gauss quadrature mentioned above, the numerical results of the first and third term on the right-hand side of the outer radial component Eq. (24) are shown in Figs. 3 and 4, where the numerical parameters are presented in Table I. It can be found in Fig. 3 that the first integral over the range from 0 to a always converges to a satisfactory precision with the maximum degree of Gauss quadrature being 70. The second integral has the same convergent behavior, but it is not presented in this paper for simplicity. However as shown in Fig. 4(a), when l, m, and n are small, the integral in the third term over the range from r to infinity cannot converge even when the degree of Gauss−Legendre quadrature is up to 200. This is unacceptable for fast calculation of sound pressure of audio sounds.

The poor integration performance of the third integral at small orders is caused by the oscillatory nature of spherical Hankel function when its argument is large.[24] To solve the problem, the scaled spherical Hankel function is introduced,

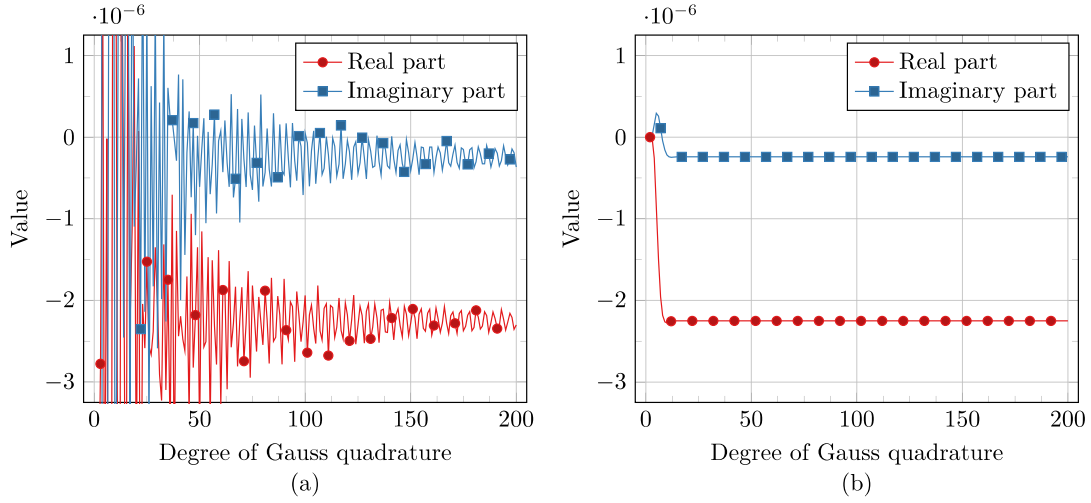

FIG. 4. (Color online) Numerical results of third term of the outer radial component of Eq. (24) when $r = a$ and $l = m = n = 0$ for (a) the direct Gauss quadrature and (b) applying the complex-plane method.

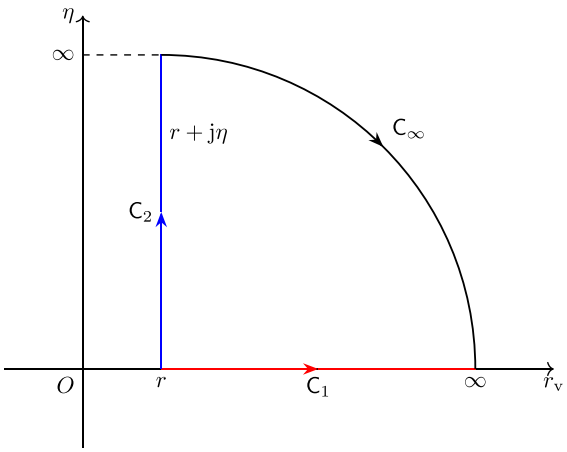

FIG. 5. (Color online) Contours of integration in the complex plane. Along C_2, $\zeta = r + j\eta$, $0 \le \eta < \infty$.

$$\hat{h}_n(x) = h_n(x)e^{-jx}, \tag{30}$$

which can be calculated by the MATLAB built-in function "besselh." By using Eq. (30), the oscillatory factor of the spherical Hankel function is extracted as e^{-jx}. The third term on the right-hand side of Eq. (24) is then rewritten as

$$F^{\mathrm{III}}_{2l,2m,2n}(r) = j_{2n}(k_a r)\left[\int_0^{k_1 a} j_{2l}(\xi)\xi d\xi\right]\left[\int_0^{k_2 a} j_{2m}(\xi)\xi d\xi\right]^* \times \int_r^{\infty} \hat{h}_{2l}(k_1 r_v)\hat{h}^*_{2m}(k_2 r_v)\hat{h}_{2n}(k_a r_v) \times e^{jk_R r_v} k_a^3 r_v^2 e^{-k_I r_v} dr_v, \tag{31}$$

by substituting the outer radial component of ultrasounds Eq. (14) into it, where $k_R = \mathrm{Re}(k_1 - k_2^* + k_a)$ and $k_I = \mathrm{Im}(k_1 - k_2^* + k_a)$. In Eq. (31), the oscillatory factor of the integrand $e^{jk_R r_v}$ varies rapidly as r_v approaches to infinity, so its numerical integration converges slowly. Equation (31) can be converted into a rapidly convergent integral by rotating the line of integration through 90° in the complex plane based on the method used in Refs. 24 and 25. It should be noted that although Eq. (31) is for the outer region as shown in Eq. (24), the results for the inner region Eq. (23) can be obtained by setting $r = a$ in Eq. (31).

As shown in Fig. 5, the variable to be integrated, r_v, is analytically continued from the real axis to the complex plane as $r_v \to r_v + j\eta$, where η is a real number.[24] The integrand in Eq. (31) is analytic in the upper half plane,[24] so its integral can be evaluated by deforming the contour. The integral along C_1 equals to the sum of the integrals along C_2 and C_∞, while C_∞ equals 0 according to Jordan's lemma (Sec. 74 in Ref. 26). Therefore, the integral Eq. (31) becomes

$$F^{\mathrm{III}}_{2l,2m,2n}(r) = j_{2n}(k_a r)\left[\int_0^{k_1 a} j_{2l}(\xi)\xi d\xi\right]\left[\int_0^{k_2 a} j_{2m}(\xi)\xi d\xi\right]^* \times j\int_0^{\infty} \hat{h}_{2l}(k_1\zeta)\hat{h}^*_{2m}(k_2\zeta)\hat{h}_{2n}(k_a\zeta) \times e^{j(k_R r - k_1\eta)} k_a^3 \zeta^2 e^{-k_R\eta - k_I r} d\eta, \tag{32}$$

where $\zeta = r + j\eta$. The highly oscillatory factor $e^{jk_R r_v}$ in Eq. (31) is then transformed into a rapid exponential decreasing factor $e^{-k_R\eta}$ in Eq. (32) as $\eta \to \infty$.

Note that the scaled spherical Hankel function $\hat{h}_n(x)$ instead of $h_n(x)$ should be used when applying Gauss–Legendre quadrature on Eq. (32) to avoid the overflow of the calculation of $h_n(x)$ when the imaginary part of x is large. Figure 4(b) shows the numerical result calculated by Eq. (32) with the same parameters used in Fig. 4(a). It can be found the integration convergence is improved using the complex plane method and the required degree of Gauss–Legendre quadrature can be decreased to 25.

IV. SIMULATIONS AND DISCUSSIONS

In this section, the numerical results for audio sounds generated by a PAL with the parameters in Table I are presented. As shown in the spherical expansion Eq. (21), the sound pressure of audio sounds can be obtained by using the threefold summation series with respect to l, m, and n

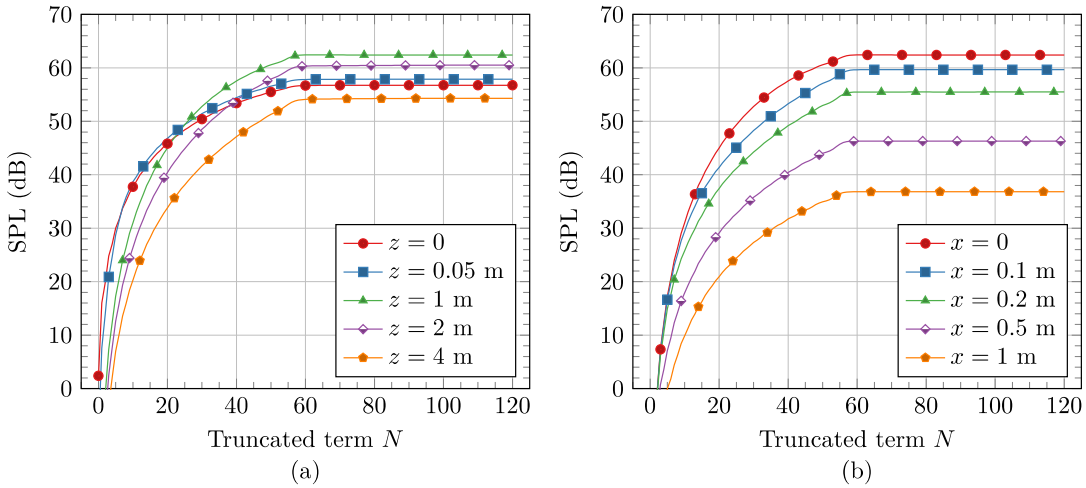

FIG. 6. (Color online) Convergence of the audio sound SPL with respect to the truncated term N for (a) the on-axis field points at $x = 0$ and (b) the off-axis field points at $z = 1$ m.

https://doi.org/10.1121/10.0001261

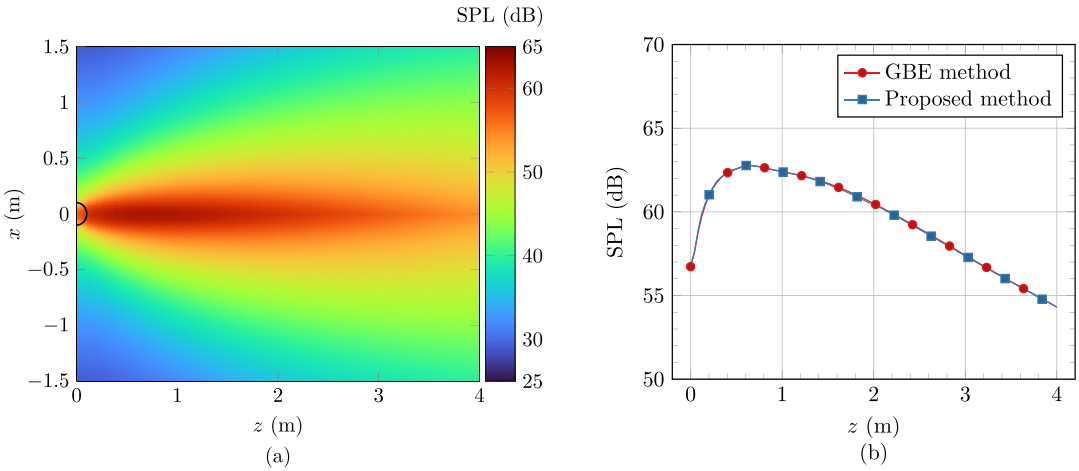

FIG. 7. (Color online) The sound fields of audio sounds generated by a PAL (a) in whole space and (b) on the radiation axis.

provided that the angular component $P_{2n}(\cos\theta)$ and the radial component Eq. (22) are obtained. The series should be truncated to obtain numerical results. The truncated term is set as N for all l, m, and n for simplicity.

Figure 6 shows the audio sound pressure level (SPL) with respect to the truncated term N for (a) the on-axis field points at $x=0$ and (b) the off-axis field points at $z=1$ m. It can be found that all curves converge as the truncated term increases. Specifically, the truncated error is less than 0.3, 0.1, and 0.01 dB when the truncated term $N=60$, $N=70$, and $N=85$, respectively. So, the results with $N=85$ are presented in the following simulations.

To illustrate the efficiency and accuracy of the proposed method, the widely used GBE method of Eq. (7) is used for comparisons.[8] The GBE parameters in Ref. 10 are adopted in this paper. For the GBE method, the field coordinate is also the integrated (virtual source) coordinate as shown in Eq. (4) which may cause singularities if the Gauss−Legendre quadrature is used, so the 1/3 Simpson's rule (Sec. 2.2 in Ref. 28) is used to calculate the numerical results of integrals of Eqs. (4) and (8). The integrated coordinates are evenly discretized, and the field coordinate is set as the middle point between adjacent integrated coordinates to avoid singularities. The infinitely large integral domain of the integral needs to be reduced to a specific region covering the major energy of ultrasound beams,[16] so the integral domain is reduced to a cylindrical column centered along the axis of the PAL with a radius of 5 m (50 times of the PAL radius) and a length of 10 m (more than four times of the effective absorption length).

Figure 7(a) shows the SPL distribution of audio sounds generated by a PAL in whole space calculated by the proposed method, which is similar to that calculated by the GBE method (not shown here for simplicity). The separation of the inner and outer regions, i.e., $r=a=0.1$ m, is plotted as a black hemi-circle in Fig. 7(a). It can be found the inner region is insignificant for PAL applications because it is very small. Therefore, only the calculation of the outer region sound fields Eq. (24) is required for most cases. Figure 7(b) shows the SPLs of audio sounds on the radiation axis, i.e., $x=0$, calculated by the two methods, are almost the same.

Table II shows the calculation time of the two methods for three typical field points. The precision criterion is to make the difference between the SPL calculated by two methods be less than 0.02 dB. The calculation time is based on a personal computer with 2.5 GHz main frequency and 16 GB random access memory. It can be seen from Table II that the calculation time of the proposed method is small and almost the same for all cases, while the one of the GBE method is at least 15 times larger.

The computation load of the GBE method is brought by the requirements of sound pressure of ultrasounds at many virtual source points and the integral over a large space, which do not occur in the proposed method. The convergence speed of the GBE method is different at different field points and it converges very slowly when the field point is close to the plane $z=0$. For example, it requires even more than 2000 s to obtain the accurate result at $x=y=z=0$ as shown in Table II. The reason is that the near field virtual sources are dominant in this case while their source density function (proportional to the ultrasounds sound pressure) varies significantly so that the integrand in Eq. (4) oscillates dramatically.[10] However, it should be noted that both solutions of Eq. (4) and Eq. (21) have limited ability to capture the nearfield sound correctly because the local nonlinear effects are neglected in the Westervelt equation. In this case, the more complex second-order nonlinear wave equation has to be used and the proposed method needs to be extended.[7] It is also noteworthy that all field coordinates of

TABLE II. Calculation time of the proposed method and GBE method.

	Calculation time (s)	
Calculated field point	Proposed method	GBE method
$x=y=0$ and $z=1$ m (on-axis)	12.1	186.1
$x=0.5$ m, $y=0$, and $z=1$ m (off-axis)	11.9	220.5
$x=y=z=0$ (nearfield)	15.2	2059.5

the proposed method shown in Eq. (21) are uncoupled so that the field in whole space can be calculated much faster for a large number of field points than the GBE method.

V. CONCLUSIONS

A simplified but rigorous expression of the quasilinear solution of the Westervelt equation for calculating the audio sounds from a circular PAL is developed in this paper. The key step is to express the Green function of a point monopole in free space by a series consisting of trigonometric, Legendre, and spherical Bessel functions, so that the fivefold integral in the expression of audio sounds generated by a PAL can be simplified to threefold summations by using the orthogonal properties of the trigonometric and Legendre functions. The proposed expression has the uncoupled angular component determined by Legendre polynomials and the radial one, which is a rapidly converged integral involving spherical Bessel functions that converge rapidly. Unlike the widely used GBE method, the proposed expansion avoids the additional Fresnel approximation and can be calculated efficiently. In the numerical simulations, the GBE method is at least 15 times slower than the proposed method and shows poor convergence in the near field while the proposed method is computationally efficient in whole space. Future work can explore fast calculation methods for rectangular PALS.

ACKNOWLEDGMENTS

This research is supported under the Australian Research Council's Linkage Project funding scheme (No. LP160100616).

[1]W. S. Gan, J. Yang, and T. Kamakura, "A review of parametric acoustic array in air," Appl. Acoust. **73**(12), 1211–1219 (2012).
[2]N. Tanaka and M. Tanaka, "Mathematically trivial control of sound using a parametric beam focusing source," J. Acoust. Soc. Am. **129**(1), 165–172 (2011).
[3]Y. Nakashima, T. Ohya, and T. Yoshimura, "Prototype of parametric array loudspeaker on mobile phone and its acoustical characteristics," in *Audio Engineering Society Convention 118*, Barcelona, Spain (2005), pp. 1–6.
[4]B. Castagnède, A. Moussatov, D. Lafarge, and M. Saeid, "Low frequency *in situ* metrology of absorption and dispersion of sound absorbing porous materials based on high power ultrasonic non-linearly demodulated waves," Appl. Acoust. **69**(7), 634–648 (2008).
[5]E. Skinner, M. Groves, and M. K. Hinders, "Demonstration of a length limited parametric array," Appl. Acoust. **148**, 423–433 (2019).
[6]M. F. Hamilton and D. T. Blackstock, *Nonlinear Acoustics* (Acoustical Society of America, New York, 2008).
[7]M. Červenka and M. Bednaøík, "A versatile computational approach for the numerical modelling of parametric acoustic array," J. Acoust. Soc. Am. **146**(4), 2163–2169 (2019).
[8]M. Červenka and M. Bednaøík, "Non-paraxial model for a parametric acoustic array," J. Acoust. Soc. Am. **134**(2), 933–938 (2013).
[9]J. Wen and M. Breazeale, "A diffraction beam field expressed as the superposition of Gaussian beams," J. Acoust. Soc. Am. **83**(5), 1752–1756 (1988).
[10]M. Červenka and M. Bednaøík, "On the structure of multi-Gaussian beam expansion coefficients," Acta Acust. Acust. **101**(1), 15–23 (2015).
[11]T. D. Mast and F. Yu, "Simplified expansions for radiation from a baffled circular piston," J. Acoust. Soc. Am. **118**(6), 3457–3464 (2005).
[12]M. A. Poletti, "Series expansions of rotating two and three dimensional sound fields," J. Acoust. Soc. Am. **128**(6), 3363–3374 (2010).
[13]M. J. Carley, "Series expansion for the sound field of a ring source," J. Acoust. Soc. Am. **128**(6), 3375–3380 (2010).
[14]M. A. Poletti, "Spherical expansions of sound radiation from resilient and rigid disks with reduced error," J. Acoust. Soc. Am. **144**(3), 1180–1189 (2018).
[15]H. Bass, L. Sutherland, and A. Zuckerwar, "Atmospheric absorption of sound: Update," J. Acoust. Soc. Am. **88**(4), 2019–2021 (1990).
[16]J. Zhong, R. Kirby, and X. Qiu, "A non-paraxial model for the audio sound behind a non-baffled parametric array loudspeaker (L)," J. Acoust. Soc. Am. **147**(3), 1577–1580 (2020).
[17]D. Huang and M. Breazeale, "A Gaussian finite-element method for description of sound diffraction," J. Acoust. Soc. Am. **106**(4), 1771–1781 (1999).
[18]H.-J. Kim, L. W. Schmerr, Jr., and A. Sedov, "Generation of the basis sets for multi-Gaussian ultrasonic beam models—An overview," J. Acoust. Soc. Am. **119**(4), 1971–1978 (2006).
[19]S. Zhang and J. Jin, *Computation of Special Functions* (Wiley, New York, 1996).
[20]H. A. Mavromatis and R. S. Alassar, "A generalized formula for the integral of three associated Legendre polynomials," Appl. Math. Lett. **12**(3), 101–105 (1999).
[21]A. Messiah, *Quantum Mechanics: Volume II* (North-Holland, Amsterdam, 1962).
[22]T. Sauer, *Numerical Analysis* (Pearson Education, New York, 2012).
[23]M. Majić and E. C. Le Ru, "Numerically stable formulation of Mie theory for an emitter close to a sphere," Appl. Opt. **59**(5), 1293–1300 (2020).
[24]K. Davies, M. Strayer, and G. White, "Complex-plane methods for evaluating highly oscillatory integrals in nuclear physics: I," J. Phys. G: Nucl. Phys. **14**(7), 961–972 (1988).
[25]D. Huybrechs and S. Vandewalle, "On the evaluation of highly oscillatory integrals by analytic continuation," SIAM J. Numer. Anal. **44**(3), 1026–1048 (2006).
[26]J. W. Brown and R. V. Churchill, *Complex Variables and Applications* (McGraw-Hill, New York, 2003).
[27]ISO 9613-1:1993. "Acoustics—Attenuation of sound during propagation outdoors—Part 1: Calculation of the absorption of sound by the atmosphere" (International Organization for Standardization, Geneva, 1993).
[28]P. F. Davis and P. Rabinowitz, *Methods of Numerical Integration* (Academic, San Diego, CA, 1984).